

19

20 The incorporation of sulfate in calcium and strontium hydroxylapatites,
21 prepared in aqueous solution at pH 9, was verified by combustion
22 analysis of sulfate, infrared and Raman spectroscopy, and by
23 determination of unit cell parameters. Sulfate could not be incorporated
24 into barium hydroxylapatite because of the preferential formation of
25 BaSO₄.

26

27 The amount of sulfate substituted in the apatite was affected by the mole
28 ratio of sulfate to phosphate in the reaction mixture and by the nature of
29 the counter ion in the sulfate reagent. When sodium is the counter ion in
30 the sulfate reagent, the molar amounts of both sodium and sulfate in the
31 product apatite can be explained by assuming charge compensation by
32 sodium ions and sulfate displacement of phosphate and calcium. With
33 lithium as the counter ion, a greater molar amount of lithium than sulfate
34 is incorporated into the apatite, an observation that requires an additional
35 charge-compensation mechanism. With potassium and rubidium as
36 counter ions, less of the counter ion is incorporated than sulfate, probably

37 a result of less favorable accommodation of the larger cation in the
38 apatite structure.
39
40 The maximum molar amount of sulfate incorporated in hydroxylapatite
41 (prepared in the presence of Na⁺) is more than three times lower than the
42 maximum molar amount of carbonate that can be incorporated, a
43 difference that can be explained by the relative solubilities of the
44 substituted apatites. The unit cell parameters determined for both
45 sulfated calcium and strontium hydroxylapatites synthesized with the
46 sodium counter ion show a slight increase in the a-axis length and a
47 nearly constant c-axis length with increasing sulfate content. The
48 difference in the variation of unit cell parameters with anion content can
49 be rationalized by the difference in size of the anion.
50
51 The results indicate that sulfate can be incorporated into biomaterials
52 such as apatite or in composites with calcium sulfate and that the design
53 of new apatites and composites could include the use of medically
54 desirable counter cations.

55

56 **Keywords:** Apatite, sulfate, incorporation of sulfate, unit cell, IR,
57 strontium apatite, sulfated apatite, calcium sulfate-apatite composite

58

59 **Introduction**

60

61 Calcium sulfate has been used as a biomaterial since the later part of the
62 19th century. It has been used to repair bone defects, augment sinuses,
63 and in a variety of dental applications (Thomas and Puleo 2008; Ricci et
64 al. 2000). Discussions of the mechanism by which this extraordinary
65 compound operates usually focus on the efficacy of its resorption and its
66 ability to initiate production of a calcium-phosphate lattice; that is, to
67 stimulate new bone growth (Ricci 2000). Increased calcium ion
68 concentrations may act as a stimulus to osteoblasts (bone-producing
69 cells) and inhibitor of osteoclast (bone-dissolving cells) activity (Thomas
70 and Puleo 2008). Calcium sulfate has been combined with organic
71 compounds such as gelatin, poly(lactic) acid, and carboxymethylcellulose,
72 as well as calcium phosphate and hydroxylapatite ($\text{Ca}_{10}(\text{PO}_4)_6(\text{OH})_2$), in

73 this work designated as CaApOH). Parsons et al. (1988) report on
74 mixtures that are “osteoconductive composite grouts for orthopedic use.”
75 Mixtures of calcium sulfate with either apatite or calcium phosphate have
76 been reported to resorb more slowly, which can have clinical advantages
77 (Parsons et al. 1988; Urban et al. 2007; Fillingham et al. 2012; Yang et al.
78 2012; Kuo et al. 2015). Because apatite has a singular ability to
79 accommodate ions by substitution, it is possible that the efficacy in bone
80 healing/renewal of calcium sulfate alone and in composites together with
81 hydroxylapatite may involve substitution of sulfate in the newly formed
82 biological apatite. Moreover, the use of sulfated apatite (SCaApOH),
83 rather than CaApOH, in mixtures with calcium sulfate may be
84 advantageous.

85
86 Among the many anions that can function as substituents in apatite,
87 carbonate has received the most attention primarily due to its presence in
88 bones and teeth. The substitution of sulfate ion, on the other hand, is
89 poorly understood. One might anticipate that on the basis of its charge,
90 sulfate would behave like carbonate and replace either phosphate (B-type

91 substitution) or the monovalent ion (A-type substitution). On the other
92 hand, its structural and electronic similarity to phosphate—sulfate and
93 phosphate are isoelectronic-- suggest that sulfate might only replace
94 phosphate, with appropriate accommodations to maintain local charge
95 neutrality in the apatite structure. The larger size of sulfate mitigates
96 against its ability to substitute for monovalent anions in the apatite
97 channels. The smaller carbonate ion, which has a volume of 28 \AA^3 (as
98 opposed to 43 \AA^3 for sulfate, both calculated from thermodynamic radii
99 (Roobottom 1999)), can replace channel hydroxide to a limited extent in
100 apatites that have estimated channel volumes of about 30 \AA^3 or less
101 (Goldenberg et al. 2015).

102
103 That sulfate can take the place of phosphate to produce compounds with
104 an apatitic stoichiometry and structure is supported by the existence of
105 “sulfate” apatites, such as $\text{Na}_6\text{Ca}_4(\text{SO}_4)_6\text{F}_2$, and $\text{Na}_6\text{Pb}_4(\text{SO}_4)_6\text{F}_2$ (Klement
106 et al. 1939; Kreidler and Hummel 1970), and compounds containing
107 both orthosilicate and sulfate, such as $\text{M}_{10}(\text{SiO}_4)_3(\text{SO}_4)_3\text{F}_2$, where M =
108 Ca, Sr, and Pb (Kreidler and Hummel 1970) occur naturally (ellestadite is

109 the F/OH end member for M = Ca, McConnell 1937; Khorari et al. 1994)
110 and also have been synthesized. A recent study of sulfate substitution in
111 hydroxylapatite, using microwave heating of the aqueous reaction
112 mixture, produced a compound whose formula was given as $\text{Ca}_{10}(\text{PO}_4)_{6-x}(\text{SO}_4)_x(\text{OH})_{2-x}$, with $x = 0.05-0.5$ (Alshemary et al. 2013). Evidence for
113 the incorporation of sulfate included X-ray diffraction and IR peak
114 broadening, as well as an increase in both the a- and c-axis lengths with
115 increased sulfate concentration in the product. Hydrothermal processing
116 of a mixture of sulfate and amorphous calcium phosphate produced
117 sulfated hydroxylapatites that showed no change in lattice parameters
118 (Toyama et al. 2013).

120

121 In order to explore the possible role of sulfate substitution in apatite as
122 part of the biocompatibility and resorbability of calcium sulfate and
123 sulfated hydroxylapatite, we report here our studies of sulfate
124 incorporation into hydroxylapatite. Because biomaterials can be
125 designed with ancillary ions that can provide additional nutrients
126 (Pasteris 2016), we have also studied the effect of the counter ion in the

127 sulfate reagent on the incorporation process. The use of selected counter
128 ions (e.g., Li^+ , Na^+ , K^+ , Zn^{2+} , Mg^{2+}) in the sulfate reagent may produce
129 apatites deliberately doped with medically desirable ions that could be
130 released during dissolution/resorption of the biomaterial. To provide
131 greater depth of understanding about substitution processes in apatite, we
132 also include our work on sulfate substitution in strontium and barium
133 hydroxylapatites.

134

135

Experimental Methods

136 Milli-Q deionized water and ACS reagent grade reagents with purities
137 above 98% were used for the preparation of all samples.

138

Syntheses

139 Sulfated calcium and strontium apatites were synthesized in a round
140 bottom flask using the following solutions: 0.33 M $\text{Ca}(\text{NO}_3)_2 \cdot 4\text{H}_2\text{O}$ or
141 0.33 M $\text{Sr}(\text{NO}_3)_2$, 0.20 M A_2SO_4 , and 0.20 M $\text{NH}_4\text{H}_2\text{PO}_4$ with A = Li,
142 Na, K, Rb. The amounts of each solution used were based on the 5:3:1

143 stoichiometry of $M_5(PO_4)_3OH$ rather than the formula (vide infra) of the
144 desired apatite. The amount of the sulfate solution was varied to provide
145 sulfate to phosphate mole ratios of 0.5 to 1 up to 4 to 1 (sulfate to
146 phosphate). In separate dropping funnels, the solutions of $NH_4H_2PO_4$ and
147 $M(NO_3)_2$ were added dropwise at 0.5 drop per second to the A_2SO_4
148 solution, magnetically stirred in a round bottom flask at 80 °C. The pH of
149 the mixture was adjusted to 9 with 3 M NH_3 after 10 drops of each
150 reagent were added. The pH of the mixture was maintained at 9 during
151 the addition and digestion periods using 3 M NH_3 . After the digestion
152 time of 24 hours, during which the reaction mixture was stirred and
153 heated, the white precipitate was suction filtered and washed 6 times
154 using Milli-Q water. The product was dried in a vacuum oven for 24
155 hours at 120 °C and 5 torr. The yields were 85-95%.

156 **Identification and Analysis**

157 All products were identified by X-ray diffraction using a PANalytical
158 X'Pert PRO Multi purpose diffractometer Theta-Theta System with Cu-
159 Ka radiation ($\lambda=1.54060 \text{ \AA}$) and analyzed using the PANalytical program

160 X'Pert Highscore Plus. Samples were prepared on a 32 mm glass slide
161 for scanning (30 minutes) with a range from 5 to 70° 2 θ .

162 IR spectra were obtained on a Bruker Tensor 37 IR Spectrometer with a
163 Ge ATR mount using 256 scans and a resolution of 2 cm⁻¹.

164 In addition to combustion analysis of sulfur (Galbraith Laboratories,
165 Knoxville TN and in-house use of a Costech ECS 4010 CHNS-O
166 system), the presence of sulfate in each apatite sample was confirmed by
167 precipitation of BaSO₄ from an acid solution (3M HNO₃) of the sulfated
168 apatite.

169 The weight percent of metal ions, phosphorus, and sulfur were obtained
170 using a SPECTRO Analytical ICP-AES SPECTROBLUE spectrometer
171 (Wavelengths (nm): Ca=422.673, P=177.495, Na=589.592, Li=670.780,
172 K=769.896, S=182.034). Calibration curves were prepared by dilution of
173 commercial standards of Ca, K, Na, Li, S, and P (1000 ppm) with 8 M
174 HNO₃. Apatites were dissolved in 8 M HNO₃ solution before analysis.
175 The errors in all elemental data are expected to be no greater than 5%.

176 Elemental composition was also obtained using X-ray fluorescence
177 spectroscopy with a Panalytical PW 2404 Vacuum Spectrometer
178 equipped with a 4kW Rh X-ray tube. Sample preparation involved
179 ignition to 1200 °C to create an anhydrous powder, followed by
180 preparation of glass discs using nine parts lithium tetraborate and one part
181 anhydrous sample material.

182 Unit cell parameters were determined from 2.5-hour XRD scans of
183 samples. Peaks were indexed following a star-quality PDF card that
184 matched the experimental pattern with the highest score. The program
185 UnitCell for OS X (Holland et al. 1997) provided an initial set of a- and
186 c-axis values that were refined by eliminating potentially deleterious
187 peaks. Unit cell parameters were also determined with the Panalytical
188 X'pert Highscore Plus (version 2.3e) program. Based on repeated
189 determinations of unit cell parameters on one compound the error is
190 estimated to be $\pm 0.001 \text{ \AA}$. The two methods produced cell parameters
191 generally within $\pm 0.001 \text{ \AA}$.

192

193 **Results and Discussion**

194

195 **Synthesis**

196 Sulfated calcium and strontium hydroxylapatites were prepared by
197 aqueous addition of reagents containing lithium, sodium, potassium, and
198 rubidium as the sulfate counter ion. The reaction of sodium sulfate with
199 calcium nitrate and ammonium dihydrogen phosphate produced sulfated
200 calcium hydroxylapatites (SCaApOH) containing 2 to 8 wt% sulfate. The
201 relationship between the weight percent sulfate in the apatite and the
202 mole ratio of sulfate to phosphate used in the reaction mixture is shown
203 in Figure 1, which indicates saturation of the apatite structure with sulfate
204 at about 8 wt% (with sodium as the sulfate counter ion). CaSO_4
205 (gypsum) was detected by Raman spectroscopy in reactions that utilized a
206 4 to 1 mole ratio of sodium sulfate to phosphate: at this mole ratio
207 formation of the slightly insoluble CaSO_4 becomes competitive with
208 continued incorporation of sulfate.

209 **Figure 1.**

210 By contrast, the maximum weight percent carbonate incorporated in
211 calcium hydroxylapatites is about 17% (Pasteris et al. 2014) (22.5% was
212 reported by LeGeros et al. 1967), indicating that a significantly greater
213 number of moles of carbonate can be incorporated in the structure. This
214 difference in the amount of anion incorporated can be attributed to the
215 greater insolubility of carbonated apatite relative to sulfated apatite, as
216 rationalized using the simple salt approximation for the solubility of
217 double salts (Yoder and Rowand 2006).

218

219 Sulfated strontium hydroxylapatites were prepared analogously, but the
220 formation of SrSO_4 was observed at mole ratios (sulfate to phosphate) of
221 0.4 to 1 and higher. The use of mole ratios of 0.1 to 1 up to 0.4 to 1
222 produced sulfated strontium hydroxylapatite with sulfate weight
223 percentages ranging from 1.2 to 2.2 (and no SrSO_4 detectable by XRD).
224 Attempts to prepare sulfated barium hydroxylapatites (SBaApOH) lead to
225 the formation of BaSO_4 even at a mole ratio of 0.1 to 1. The change in
226 the amount of sulfate incorporated in the alkaline earth apatites is likely
227 due primarily to the decrease in solubility of the sulfate salts (K_{sp} CaSO_4 ,

228 10^{-5} ; SrSO_4 , 10^{-7} ; BaSO_4 , 10^{-10}), which are formed in the reaction
229 mixtures.

230

231 **Composition**

232 Powder X-ray diffraction patterns of the sulfated apatites (SCaApOH)
233 were in good agreement with the pattern for CaApOH (PDF 98-002-
234 2060) and showed no appreciable change in line widths with increased
235 incorporation of sulfate. The wt% Na and SO_4 of selected calcium
236 hydroxylapatites prepared with sodium sulfate present in the reaction
237 mixture are shown in Table 1. The samples are arranged in order of
238 increasing wt% SO_4 , and it is clear that the wt% Na increases in the same
239 order. Indeed, the number of moles of sodium is roughly the same as that
240 of sulfate. Thus, the incorporation of sulfate is accompanied by the
241 incorporation of sodium.

242

243 **Table 1.** Weight percent of sodium and sulfate in selected sulfated
244 calcium hydroxylapatites prepared using sodium sulfate.

Sample	Wt% Na	Wt% SO ₄
1	0.02	0.04
2	0.07	1.69
3	0.93	2.79
4	1.13	3.90
5	1.22	4.19
6	1.68	5.51
7	1.95	6.47

245

246

247 A formula for the sulfated hydroxylapatites may be determined from the
248 relationship between the number of moles of calcium and sulfate and the
249 number of moles of alkali metal counter ions in each of the
250 hydroxylapatites. These relationships appear in Figures 2 and 3. Figure 2
251 shows an inverse 1 to 1 relationship between calcium and sulfate ions:

252 substitution of sulfate is accompanied by a loss of calcium ions. With the
253 number of moles of calcium normalized to 10 for the compound with
254 zero moles of sulfate (where the formula of the compound should be
255 $\text{Ca}_{10}(\text{PO}_4)_6(\text{OH})_2$) the intersection of the extrapolated line in Figure 2
256 with the x-axis suggests that a limiting sulfated hydroxylapatite prepared
257 with sodium as the counter ion may contain three moles of sulfate and
258 seven moles of calcium.

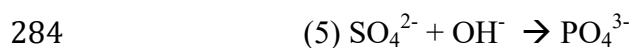
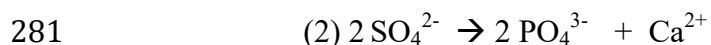
259 **Figure 2.**

260 Figure 3 shows the relationship between moles of sulfate and the moles
261 of alkali metal counter ion (present in the sulfate reactant) incorporated.
262 This reactant in most cases was Na_2SO_4 , but in five reactions Li_2SO_4 was
263 used, and in five K_2SO_4 was one of the reactants (Rb_2SO_4 was also
264 employed to confirm observations, *vide infra*). It is well known that Na^+
265 can be incorporated into the apatite lattice. Limited substitution of Li, Na,
266 and K for calcium has been reported (Simpson 1968; Mayer et al. 1983;
267 Fleet and Liu 2007; Whyte et al. 2008; Zyman et al. 2013; Yoder et al.
268 2016).
269

270 **Charge-compensation**

271 The presence of the counter ion in the apatite structure, presumably as
272 replacements for some of the Ca(2) cations in the apatite channel (Pan
273 and Fleet, 2002), is to be expected given the charge compensation
274 necessary for substitution of a -2 anion (SO_4^{2-}) for a -3 anion (PO_4^{3-}).
275 De Maeyer et al. (1996) provide six fundamental substitution schemes for
276 carbonate substitution, of which five are pertinent to B-type substitution.
277 These are rewritten below for sulfate substitution and without designation
278 of vacancies (M represents the counter ion):

279



285

286 Although our reactions were carried out at pH 9, scheme (5) is probably
287 not likely and was not observed in the extensive study of De Maeyer et al.

288 (1996). De Maeyer et al. (1996) found that schemes (1) and (2) were
289 predominantly employed in their synthetic methods using sodium and
290 potassium salts to synthesize carbonated apatites. It is important to realize
291 that the charge compensation scheme used during the synthesis is
292 dependent on the reagents and conditions. The stoichiometry of the
293 product apatite also may be best explained by a combination of charge
294 compensation schemes.

295

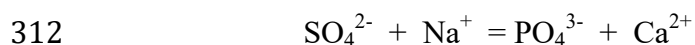
296 Interestingly, each of the alkali metal cations has its own relationship (Fig.
297 3) to sulfate content, with the lines for all three counter ions extrapolating
298 to close to zero at 0 moles of sulfate. The slopes of the lines are very
299 different, presumably a result of a change in charge compensation
300 mechanism and/or stereo-structural constraints. The relationship between
301 moles of counter ion and moles of SO_4^{2-} incorporated is approximately 1
302 to 1 for Na^+ , less than 1 for K^+ , and greater than 1 for Li^+ . In other words,
303 the incorporation of, say, 0.05 mole of sulfate is accompanied by the
304 incorporation of roughly the same amount of Na^+ , about 0.01 mole of K^+
305 and almost 0.1 mole of Li^+ .

306 **Figure 3.**

307

308 The charge balance mechanism for the sulfated hydroxylapatites made
309 with sodium as the counter ion is therefore almost surely the replacement
310 of one calcium ion by one sodium ion (scheme 3):

311



313

314 This relationship is similar to that found by Montel et al. (1981) for
315 carbonated hydroxylapatites. Thus, the formula of the sulfated
316 hydroxylapatites precipitated in the presence of sodium ion can be written
317 as $\text{Ca}_{10-x}(\text{Na})_x(\text{PO}_4)_{6-x}(\text{SO}_4)_x(\text{OH})_2$, where x = moles sulfate,. For the
318 limiting apatite containing 3 moles of sulfate (vide supra) the formula is
319 $\text{Ca}_7\text{Na}_3(\text{PO}_4)_3(\text{SO}_4)_3(\text{OH})_2$, which contains 30% sulfate and cannot be
320 prepared using our experimental procedure.

321

322 Because the sulfated hydroxylapatites prepared using lithium sulfate
323 contain more than twice as much lithium as sulfate, the charge balance

324 mechanism cannot be expressed using only schemes (1), (2), or (3). The
325 addition of scheme (4), the independent incorporation of Li^+ , is necessary
326 and also requires removal of calcium and hydroxide ions.



328 Enhanced uptake of lithium in the synthesis of carbonated apatites was also
329 reported by Mayer et al. (1986). In the IR spectra (Figure 4) of the lithium
330 sulfate incorporated apatites, the OH peak at 3570 cm^{-1} decreases as the
331 amount of sulfate increases, consistent with the operation of schemes (1) or
332 (4).

333 **Figure 4.**

334

335 For those apatites sulfated using K_2SO_4 , considerably less K^+ is present
336 than required by scheme (3). For these compounds most of the sulfate
337 incorporation occurs via scheme (1) or (2). The small amount of
338 potassium in the sulfated apatites is contrary to the composition of
339 carbonated apatites containing potassium prepared at high temperatures
340 where the mole ratio of potassium and carbonate is close to 1 to 1
341 (Verbeeck et al. 1995). It is also clear from Figure 3 that the amount of

342 sulfate incorporated when the counter ion is potassium is two to three
343 times smaller than the amount incorporated with Na as counter ion. Thus,
344 some sulfate may be incorporated with simultaneous incorporation of
345 potassium (scheme (3)) but most of the sulfate enters through the
346 operation of schemes (1) or (2). Because the total amount of sulfate is
347 low, this observation indicates that the use of scheme (1) or (2)
348 contributes a smaller amount to charge-compensation than does scheme
349 (3) when lithium and sodium are the counter ions.

350

351 The relatively minor incorporation of K^+ suggests that larger cations may
352 not easily be incorporated into the apatite structure. This observation is
353 supported by the even smaller molar amounts of rubidium found in
354 $SCaApOH$ prepared using Rb_2SO_4 . For the apatite prepared using the
355 largest mole ratio of 3 to 1 (sulfate to phosphate) only 0.04 wt% Rb was
356 found compared to 0.2 wt% K in an apatite prepared using a similar mole
357 ratio (this corresponds to the incorporation of about a tenth as many
358 moles of Rb as K). It is worth noting that the molar amount of alkali
359 metal ions incorporated follows the trend $Li^+ > Na^+ > K^+ > Rb^+$, which is

360 the inverse order of their 6-coordinate ionic radii. Both K^+ (1.38 Å) and
361 Rb^+ (1.52 Å) are significantly larger than Ca^{2+} (1.00 Å).

362

363 **IR and Raman spectra**

364 The presence of incorporated sulfate in both CaApOH and SrApOH
365 samples was confirmed by IR and Raman spectra. The Raman spectrum
366 of SSrApOH containing 4 wt% sulfate contains a peak at 1004 cm^{-1} ,
367 consistent with the sulfate symmetric stretching (ν_1) peak at 1008 cm^{-1} in
368 gypsum, as well as a peak at 3570 cm^{-1} for the OH stretch (Fig. 5). These
369 assignments are consistent with those of Pasteris et al. (2014) for the OH
370 stretch and Liu et al. (2009) for the symmetric sulfate (ν_1) stretching
371 mode. IR spectra for four SCaApOH samples prepared using various
372 mole ratios of sulfate to phosphate show an increase in the asymmetric
373 sulfate stretching (ν_3) peak intensity at ca. 1100 cm^{-1} consistent with an
374 increase in sulfate content (Fig. 6).

375 **Figure 5**

376 **Figure 6**

377

378 **Unit cell parameters**

379 Additional evidence for the incorporation of sulfate into the apatite
380 structure comes from the relationship between wt% sulfate and the unit
381 cell axial lengths (Fig. 7). The increase in the a-axis length over a range
382 of 2 wt% sulfate is about 0.015 Å. The increase in a-axis length is not
383 consistent with the thermodynamic radius of sulfate (2.18 Å, Roobottom
384 et al., 1999) relative to that of phosphate (2.47 Å, derived from the
385 apatite-appropriate volume of 0.063 nm³, Flora et al. 2004) but is
386 consistent with Dasent's values (Dasent 1982) of 2.58 Å for sulfate and
387 2.38 Å for phosphate as well as the ion volumes of 0.091 nm³ for sulfate
388 (Marcus et al. 2002) and 0.063 nm³ for phosphate (Flora et al. 2004). An
389 increase in a-axis length (as well as the c-axis length) was also observed
390 by Alshemary et al. (2013), whereas Toyama et al. (2013) found no
391 change in axial lengths.

392
393 The variation in axial lengths was also determined for a series of sulfated
394 strontium hydroxylapatites using four samples prepared with Na₂SO₄ at
395 low mole ratios (0.1 to 1 up to 0.4 to 1) and two obtained at higher mole

396 ratios where SrSO₄ was also present as a separate phase. These axial
397 lengths (Fig. 8) show the same increase in a-axis with percent sulfate
398 observed for the calcium analogs (Fig. 7).

399 **Figure 8.**

400

401

Implications

402 Our study reveals that sulfate can be incorporated into CaApOH, that the
403 sulfated apatites can be identified by IR spectroscopy, and that the
404 crystallite size, at least as indicated by XRD line widths, does not vary
405 significantly with increased incorporation of sulfate. The lattice
406 parameters for the sulfated apatites are similar to those of CaApOH, but
407 the a-axis length increases with an increase in wt% sulfate.

408

409 Because on the recognition of the therapeutic properties of calcium
410 sulfate in bone healing and reconstruction, it is reasonable to assume that
411 the incorporation of sulfate in apatite should be explored in creating new
412 biomaterials using sulfated calcium apatite alone or in a composite with
413 calcium sulfate. Sulfation of apatite may also be involved in creating

414 new bone material using calcium sulfate and calcium sulfate-
415 phosphate/apatite composites.

416

417 Because the counter ion of the sulfate reagent is incorporated into the
418 apatite, to an extent dependent on the size of the ion and the ratio of the
419 reagent to phosphate, the ions present in the sulfate reactant can be
420 tailored to produce beneficial effects on the bone mineral (LeGeros et al.
421 2009; Shepherd and Best 2011; Shepherd, et al. 2012). Substituted
422 apatites generally have a greater solubility than the parent apatite,
423 potentially increasing their resorbability and biocompatibility.

424

425 Although the solubility of sulfated apatite has not yet been determined, it
426 is likely that sulfated apatite is more soluble than carbonated apatite
427 (Yoder and Rowand 2006), but it contains a substituent (the sulfate ion)
428 that is the conjugate base of a strong acid, whereas carbonate is the
429 conjugate base of a weak acid. This difference in basicity of the
430 substituent ion may affect the solubility of the substituted apatite as a

431 function of pH, which is likely to be related to bioresorption of the apatite
432 (Arnett 2008).

433

434 More generally, our work shows that the extent of sulfation (and, perhaps,
435 most substitutions in the apatite structure) depends on the nature of the
436 counter ion in the sulfate reactant. We also suggest that the size of the
437 substituent determines the type of substitution (A- vs B-type) and the
438 relative solubilities of the substituted apatite (SCaApOH vs CCaApOH).

439

440

441 **Acknowledgements**

442 The authors are indebted to the Camille and Henry Dreyfus Foundation
443 for a Senior Scientist Mentor award (CHY) and to the Lucille and
444 William Hackman Program at Franklin & Marshall College for funding.

445 This material is based upon work supported by the National Science
446 Foundation under Grant No. 0923224. The authors gratefully
447 acknowledge helpful conversations and the acquisition of Raman spectra
448 by Jill D. Pasteris at Washington University, St. Louis, MO, and sulfur

449 analyses by Karen Mertzman and XRF analyses by Stanley Mertzman at
450 Franklin & Marshall College.

451

452

453 **References**

454

455 Alshemary, A.Z., Goh, Y-F., Akram, M., Razali, I.R., Kadir, M.R.A.,
456 Hussain, R. (2013) Microwave assisted synthesis of nano sized sulphate
457 doped hydroxyapatite. Materials Research Bulletin, 48, 2106-2110.

458

459 Arnett, T.R. (2008) Extracellular pH regulates bone cell function. The
460 Journal of Nutrition, 138, 4155-4185.

461

462 Dasent, W.E. Inorganic Energetics, 2nd edition, Cambridge University
463 Press, NY, 1982.

464

- 465 De Maeyer, E.A.P., Berbeeck, R.M.H., Pieters, I.Y. (1996) Carbonate
466 and alkalimetal incorporation in calciumhydroxyapatite, Trends in
467 Inorganic Chemistry, 4, 157-171.
- 468
- 469 Fillingham, Y.A., Lenart, B.A., Gitelis, S. (2012) Function after injection
470 of benign bone lesions with a bioceramic, Clinical Orthopaedics and
471 Related Research 470, 2014-2020.
- 472
- 473 Fleet, M.E. and Liu, X. (2007) Coupled substitution of type A and B
474 carbonate in sodium-bearing apatite. Biomaterials, 28, 916-926.
- 475
- 476 Flora, N.J., Yoder, C.H., Jenkins, H.D.B. (2004) Lattice energies of
477 apatites and the estimation of $\Delta H_f^0(\text{PO}_4^{3-}, \text{g})$. Inorganic Chemistry, 43,
478 2340-2345.
- 479
- 480 Goldenberg, J.E., Wilt, Z., Schermerhorn, D.V., Pasteris, J.D., and Yoder,
481 C.H. (2015) Structural effects on incorporated water in carbonated
482 apatites. American Mineralogist, 100, 274-280.

- 483
- 484 Holland, T.J.B., Redfern, S.A.T. (1997) Unit cell refinement from
485 powder diffraction data: the use of regression diagnostics. *Mineralogical*
486 *Magazine*, 61, 65-77.
- 487
- 488 Khorari, S., Cahay, R., Rulmont, A., Tarte, P. (1994) The coupled
489 isomorphic substitution $2(\text{PO}_4)^{3-} \rightarrow (\text{SO}_4)^{2-} + (\text{SiO}_4)^{4-}$ in synthetic apatite
490 $\text{Ca}_{10}(\text{PO}_4)_6\text{F}_2$: a study by X-ray diffraction and vibrational spectroscopy.
491 *European Journal of Solid State Inorganic Chemistry*, 31, 921-934.
- 492
- 493 Klement, R. (1939) Natrium-Calcium-sulfatapatit $\text{Na}_6\text{Ca}_4(\text{SO}_4)_6\text{F}_2$.
494 *Naturwissenschaften*, 27, 568.
- 495
- 496 Kreidler, E.R., Hummel, F.A. (1970) The crystal chemistry of apatite:
497 structure fields of fluor- and chlorapatite. *American Mineralogist*, 55,
498 170-184.
- 499

- 500 Kuo, T.F., Lee, S.Y., Wu, H.D., Porna, M., Wu, Y.W., Yang, J.C. (2015)
501 An in vivo swine study for xeno-grafts of calcium sulfate-based bone
502 grafts with human dental pulp stem cells(hDPSCs)., Materials Science
503 and Engineering,C. Materials of Biological Applications 10, 19-23.
504
505 LeGeros, R.Z., Trautz, O.R., LeGeros, J.P., Klein, E., Shirra, W.P. (1967)
506 Apatite crystallites: effects of carbonate on morphology, Science, 155,
507 1409-1411.
508
509 LeGeros, R.Q., Ito, A., Ishikawa, K., Sakae, R., and LeGeros, J.P. (2009)
510 Fundamentals of hydroxyapatite and related calcium phosphates. In B.
511 Basu, D. Katii, and A. Kumar, Eds., Advanced Biomaterials:
512 Fundamentals, Processing, and Applications, p. 19-52, Wiley, New York.
513
514 Liu, Y. Wang, A., Freeman, J.J. (2009) Raman, MIR, and NIR
515 spectroscopic study of calcium sulfates: gypsum, bassanite, and anhydrite,
516 40th Lunar and Planetary Science Conference, 2128.pdf
517

- 518 Marcus, Y, Jenkins, H.D.B., Glasser, L. (2002) Ion volumes: a
519 comparison. Journal of the Chemical Society, Dalton Transaction, 3795-
520 3798.
- 521
- 522 Mayer, I., Berger, U., Markitziu, A. and Gedalia, I. (1986) The uptake of
523 lithium ions by synthetic carbonated hydroxyapatite. Calcified Tissue
524 International, 38, 293-295.
- 525
- 526 McConnell, D. (1937). The substitution of SiO_4^{4-} and SO_4^{2-} groups for
527 PO_4^{3-} groups in the apatite structure; ellestadite, the end-member.
528 American Mineralogist, 22, 977-986.
- 529
- 530 Montel, G., Bonel, G., Heughebaert, J.C., Trombe, J.C., Rey, C. (1981)
531 New concepts in the composition, crystallization and growth of the
532 mineral component of calcified tissues. Journal of Crystal Growth, 53,
533 74-99.
- 534

- 535 Pan, Y., Fleet, M.E. (2002) Compositions of the apatite-group minerals:
536 substitution mechanisms and controlling factors, *Reviews in Mineralogy*
537 and *Geochemistry* (ed. Kohn, M. Rakovan, J., Huighes, J.M.), 48, 13-49.
538
- 539 Parsons, J.R., Ricci, J.L., Alexander, H.J., Bajpai, P.K. (1988)
540 Osteoconductive Composite Grouts for Orthopedic Use, *Annals of the*
541 *New York Academy of Sciences*, 100B, 1911-1921.
542
- 543 Pasteris, J.D. (2016) A mineralogical view of apatitic biomaterials.
544 *American Mineralogist*, 101, 2594-2610.
545
- 546 Pasteris, J.D., Yoder, C.H., Wopenka, B. (2014) Molecular water in
547 nominally unhydrated carbonated hydroxylapatite: The key to a better
548 understanding of bone mineral, *American Mineralogist*. 99, 16-27.
549
- 550 Ricci, J.L., Alexander, H. Nadkarni, P., Hawkins, M., Turner, J.,
551 Rosenblum, S., Brezenoff, L., DeLeonardis, D., Pecora, G. (2000)

552 Biological Mechanisms of Calcium-Sulfate Replacement by Bone. In J.E.
553 Davies, ed., Bone Engineering, Toronto, EM2 Inc., pp. 332-344.
554
555 Roobottom, H.K., Jenkins, H.D.B., Passmore, J., Glasser, L. (1999)
556 Thermochemical radii of complex ions. Journal of Chemical Education,
557 76, 1570-1573.
558
559 Shepherd, J.H., Shepherd, D.V., Best, S.M. (2012) Substituted
560 hydroxyapatites for bone repair. Journal of Materials Science Materials in
561 Medicine, 23, 2335-2347.
562
563 Simpson, D.R. (1968) Substitutions in apatite: I. Potassium-bearing
564 apatite. American Mineralogist, 53, 432-444.
565
566 Thomas, M.V. and Puleo, D.A. (2009) Calcium sulfate: Properties and
567 clinical applications. Journal of Biomedical Materials research Part B
568 88B, 597-610
569

- 570 Toyama, T., Kameda, S. Nichimiya, N. (2013) Synthesis of sulfate-ion-
571 substituted hydroxyapatite from amorphous calcium phosphate.
572 Bioceramics Development and Applications, S1: 011. doi: 10.4172/2090-
573 5025.S1-011
574
575 Urban, R.M., Turner, T.M., Hall, D.J., Inoue, N., Gitelis, S. (2007)
576 Increased bone formation using a calcium sulfate and calcium phosphate
577 composite graft, Clinical Orthopaedics and Related research, Clinical
578 Orthopaedics and Related Research 459, 110-117.
579
580 Verbeeck, R.M.H., De Maeyer, E.A.P., Driessens, F.C.M. (1995)
581 Stoichiometry of potassium- and carbonate-containing apatites
582 synthesized by solid state reactions. Inorganic Chemistry 34, 2084-2088.
583
584 Whyte, J., Hadden, D.J., Gibson, I.R. and Skakle, J.M.S. (2008)
585 Synthesis and stability of potassium/carbonate co-substituted
586 hydroxyapatites. Key Engineering Materials, 361-363, 207-210.
587

588

589 Yang, H.L., Zhu, X.S., Chen, L. Chen, C.M. Mangham, D.C., Coulton, L.A.,
590 and Aiken, S.S. (2012) Bone healing response to a synthetic calcium
591 sulfate/tricalcium phosphate graft material in a sheep vertebral body
592 defect model. Biomedical Material Research B. Applied Biomaterials,
593 100B, 1911-1921.

594

595 Yoder, C.H., Landes, N.R., Tran, L.K., Smith, A.K., and Pasteris, J.D.
596 (2016) The relative stabilities of A- and B-type carbonate substitution in
597 apatites synthesized in aqueous solution, Mineralogical Magazine,
598 preproof accepted article, DOI: 10.1180/minmag.2016.080.035.

599

600 Yoder, C.H., Rowand, J.P. (2006) Application of the simple salt lattice
601 energy approximation to the solubility of minerals. American
602 Mineralogist, 91, 747-752.

603

604 Zyman, Z.Z. and Tkachenko, M.V. (2013) Sodium-carbonate co-
605 substituted hydroxyapatite ceramics. Processing and Application of

606 Ceramics, 7, 153-157.

607

608

609 **Tables:**

610

611 **Table 1.** Weight percent of sodium and sulfate in selected sulfated
612 calcium hydroxylapatites prepared using sodium sulfate.

Sample	Na ⁺	SO ₄ ²⁻
1	0.02	0.04
2	0.07	1.69
3	0.93	2.79
4	1.13	3.90
5	1.22	4.19
6	1.68	5.51
7	1.95	6.47

613

614 **List of Figure captions:**

615

616 **Figure 1.** The wt% sulfate incorporated into CaApOH as a function of
617 the mole ratio of sulfate to phosphate in the reaction mixture with sodium
618 as counter ion.

619

620 **Figure 2.** Relationship between calcium content and amount of sulfate
621 incorporated in calcium hydroxylapatites with sodium as counter ion.

622

623 **Figure 3.** Relationship between sulfate and counter cation content.

624 Squares = Li, diamonds = Na, triangles = K.

625

626 **Figure 4.** The OH region of the IR spectra of several SCaApOH apatites
627 prepared using lithium as the counter ion. Spectra normalized to the ν_3
628 phosphate band.

629

630 **Figure 5.** The Raman spectra of the phosphate and sulfate stretching
631 regions of top, SSrApOH showing the ν_1 phosphate stretch at 948 cm^{-1}
632 and the ν_1 sulfate stretch at 1000 cm^{-1} , middle, gypsum (1008 cm^{-1}) and,
633 bottom, non-sulfated CaApOH (Sigma-Aldrich).

634

635 **Figure 6.** The 960 to 1200 cm^{-1} region of the IR spectra in SCaApOH
636 samples containing varying amounts of sulfate. The peak at 1030 cm^{-1} is
637 the ν_3 P-O stretching band; the peak at ca. 1100 cm^{-1} is the ν_3 S-O
638 stretching band.

639

640 **Figure 7.** The effect of incorporated sulfate on the unit cell a- and c-
641 axial lengths for SCaApOH synthesized using sodium as the counter ion.
642 The a-axis is represented by triangles and the c-axis by circles.

643

644 **Figure 8.** Variation of unit cell axial lengths with sulfate percentage for
645 SSrApOH. The a-axis is represented by triangles and the c-axis by
646 circles.

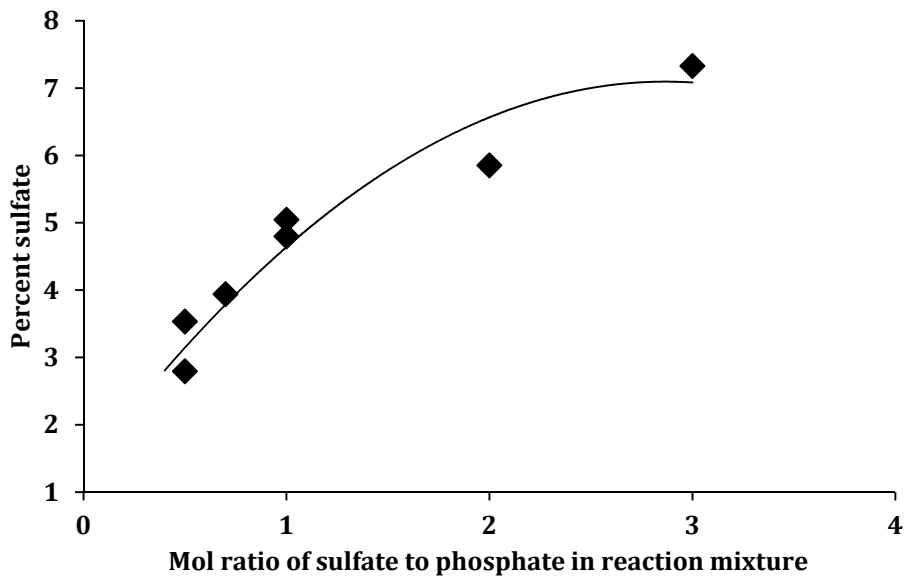
647

648

649 **Figures:**

650

651 **Figure 1**

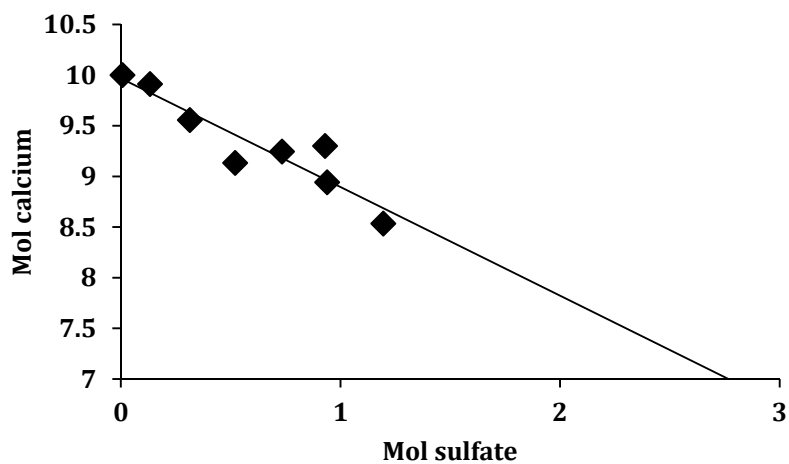


652

653

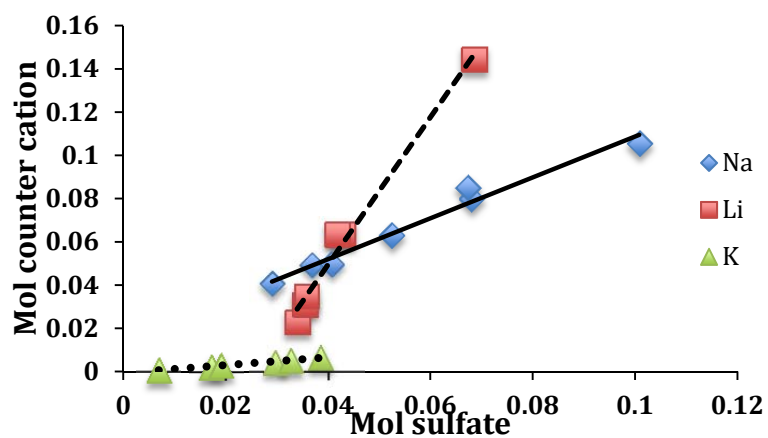
654

655 **Figure 2**



656

657 **Figure 3**



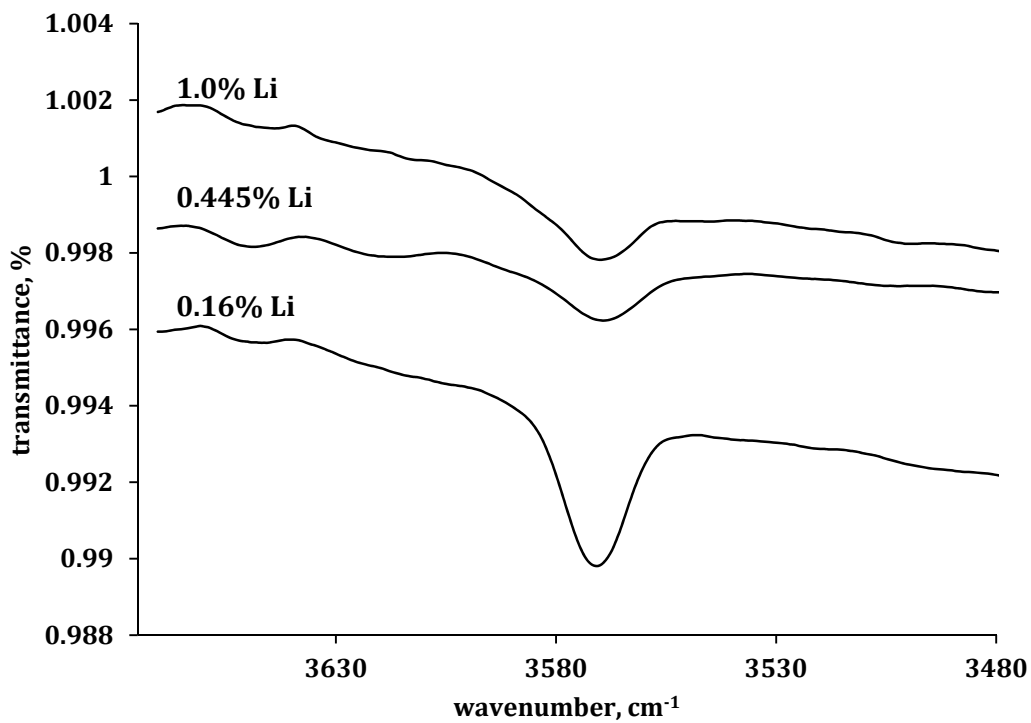
658

659

660

661 **Figure 4**

662

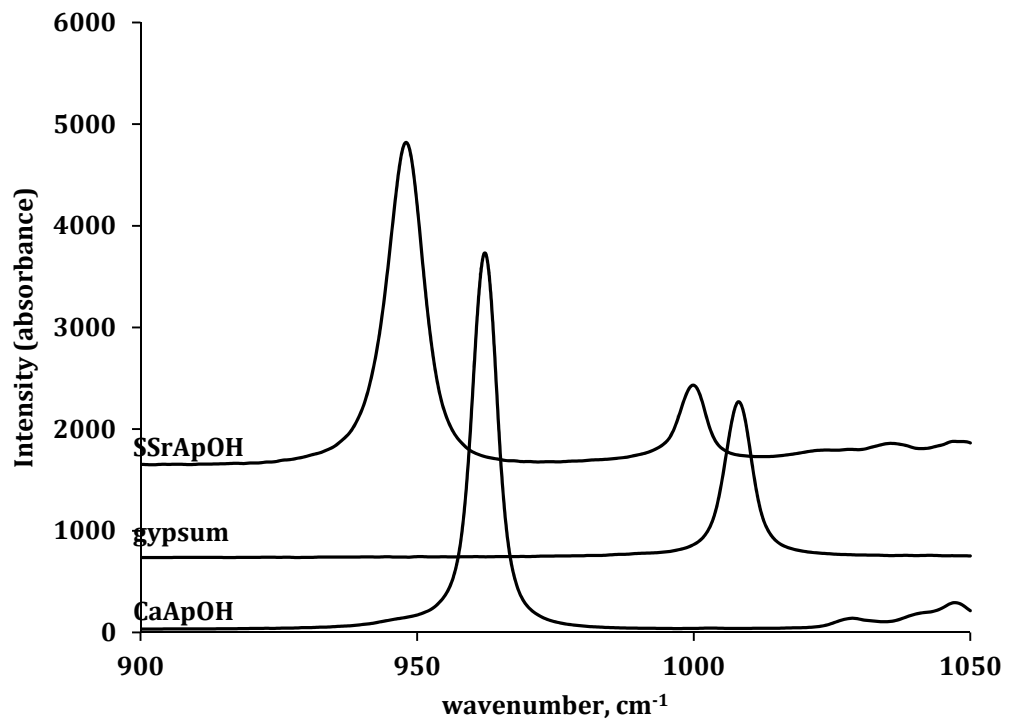


663

664

665 **Figure 5**

666



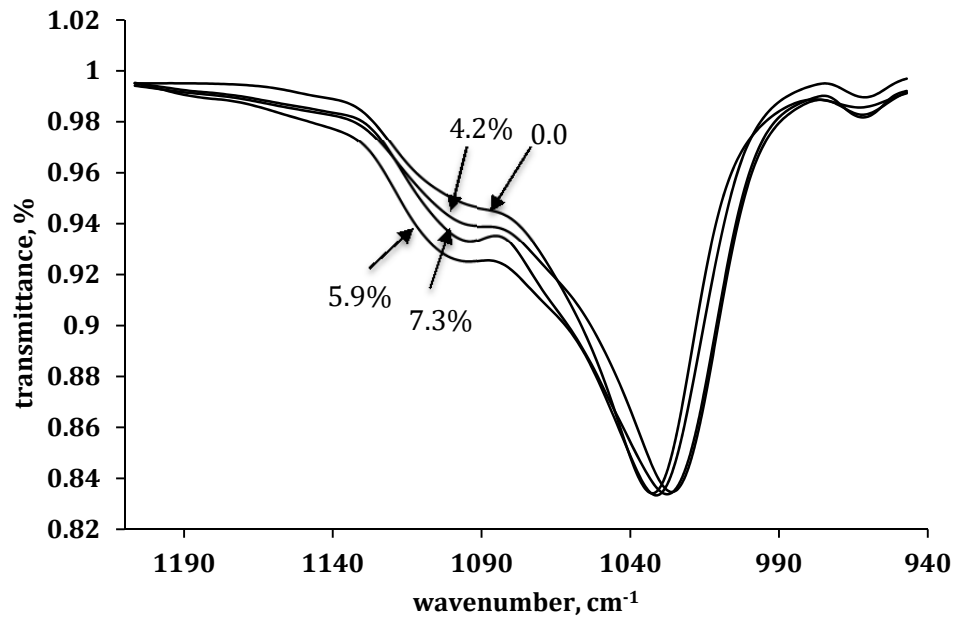
667

668

669

670

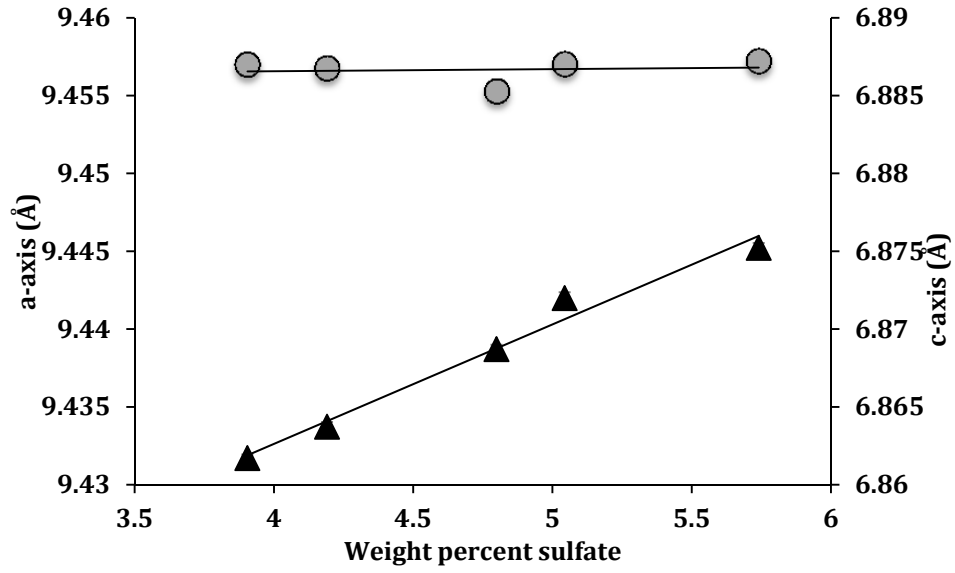
671 **Figure 6**



672

673

674 **Figure 7**

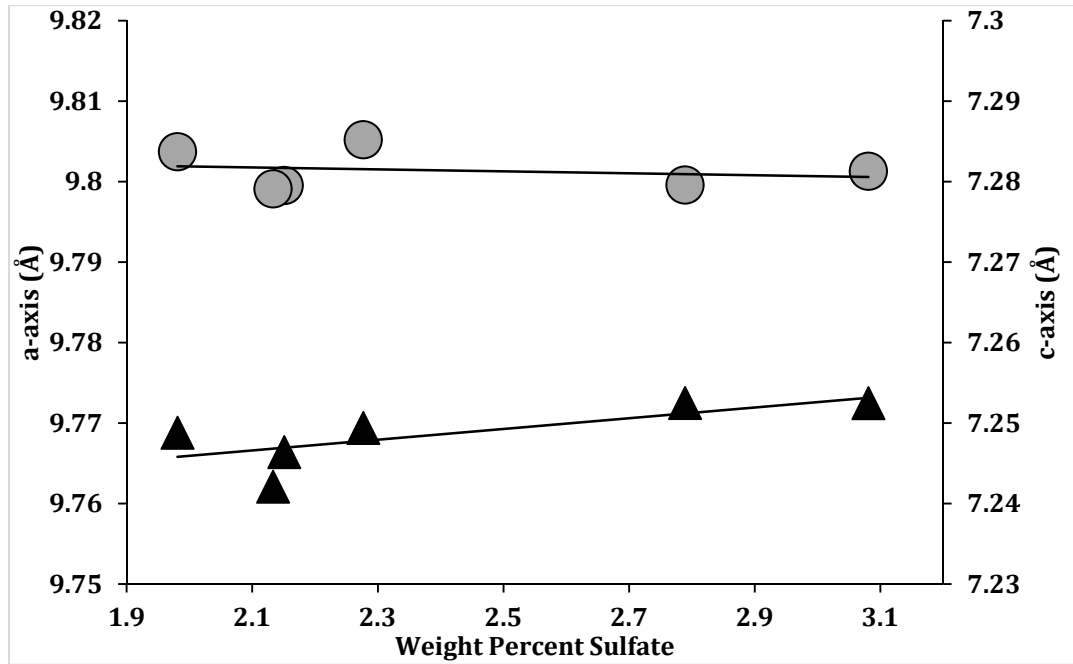


675

676

677

678 **Figure 8**



679

680